ISSN Print: 0976-6340 ISSN Online: 0976-6359

INTERNATIONAL JOURNAL OF MECHANICAL ENGINEERING & TECHNOLOGY (IJMET)

https://iaeme.com/Home/journal/IJMET

High Quality Peer Reviewed Refereed Scientific, Engineering & Technology, Medicine and Management International Journals

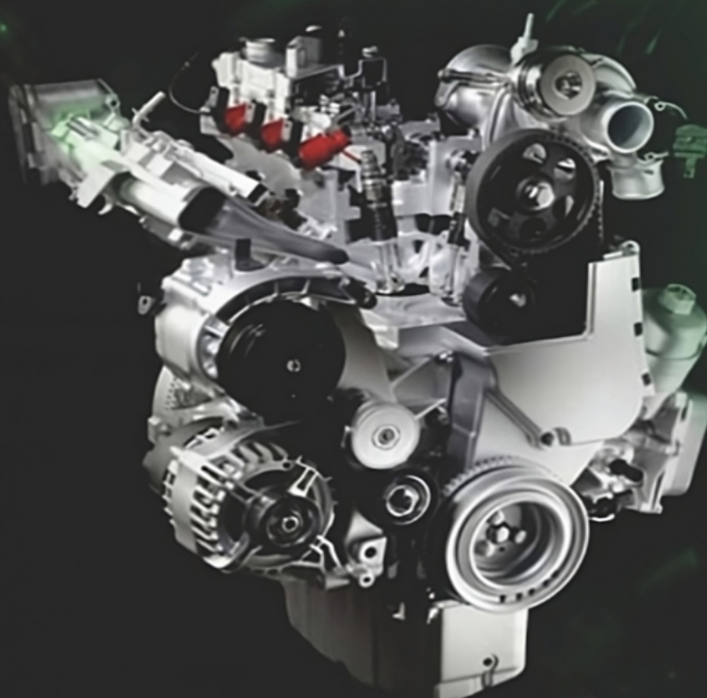

PUBLISHED BY

IAEME Publication
Chennai, Tamilnadu, India
Mobile: +91-9884798314, 7358208318
E-mail: iaemedu@gmail.com, editor@iaeme.com

International Journal of Mechanical Engineering and Technology (IJMET)
Volume 16, Issue 3, May-June 2025, pp. 88-105, Article ID: IJMET_16_03_005
Available online at https://iaeme.com/Home/issue/IJMET?Volume=16&Issue=3
ISSN Print: 0976-6340; ISSN Online: 0976-6359; Journal ID: 4544-4179
Impact Factor (2025): 20.99 (Based on Google Scholar Citation)
DOI: https://doi.org/10.34218/IJMET_16_03_005

THERMAL SIMULATION OF LFP BATTERY MODULE DURING CHARGING AND DISCHARGING CYCLES USING CFD

Karthik A V [1], Balaji S [1], Venkat S G [1], Muralidhar Reddy [1]

[1] SOLIZE India Technology Private Limited, Bangalore, India.

ABSTRACT

Efficient thermal management of lithium iron phosphate (LFP) batteries is essential to enhance safety and performance in electric vehicle and stationary storage applications. This study presents a detailed CFD-based thermal simulation of a 23-cell battery module during charging and discharging cycles using Cradle SCStream. Heat generation is analytically estimated based on internal resistance, and simulations capture thermal gradients, heat flow, and temperature evolution over time. Simulation results reveal critical insights into the thermal performance of LFP cells under different operating currents.

Keywords: Battery thermal management, LFP battery, CFD, Charging, Discharging, Heat generation.

Cite this Article: Karthik A V, Balaji S, Venkat S G, Muralidhar Reddy. (2025). Thermal Simulation of LFP Battery Module During Charging and Discharging Cycles Using CFD. *International Journal of Mechanical Engineering and Technology (IJMET)*, 16(3), 88-105.

https://iaeme.com/MasterAdmin/Journal_uploads/IJMET/VOLUME_16_ISSUE_3/IJMET_16_03_005.pdf

1. Introduction

The demand for high-performance lithium-ion batteries, particularly LFP (LiFePO4) cells, has grown due to their thermal stability, safety, and long cycle life. However, during charge and discharge operations, internal resistance results in heat generation, which can impact battery performance and longevity. Accurate prediction of temperature evolution within battery packs is crucial to designing effective thermal management systems (TMS).

CFD tools have increasingly been adopted to analyze the complex thermal behaviors of batteries. Studies such as Rao et al. (2014) and Wang et al. (2021) have highlighted the influence of design parameters, cooling strategies, and material properties on battery pack thermal profiles. Yet, specific investigation into single-module LFP packs under realistic 1C/0.6C operations remains limited. This paper aims to bridge that gap through a rigorous thermal analysis using experimentally validated parameters.

2. Literature Review

Several researchers have addressed the importance of thermal 89odelling in battery systems:

- Rao et al. (2014) investigated passive and active TMS using CFD and found that natural convection is often insufficient for high C-rate applications.
- Al-Zareer et al. (2018) developed a detailed electro-thermal model for LFP batteries and validated it using thermal imaging and sensor data.
- Wang et al. (2021) analyzed thermal behavior of cylindrical and prismatic cells under various configurations and emphasized the importance of cell interconnection on heat generation.
- Kim et al. (2017) performed experimental and numerical investigation of a passive air cooling system for lithium-ion batteries, showing that optimized air channels can reduce hotspot formation.
- Yang et al. (2018) developed a coupled electro-thermal model for prismatic lithium-ion batteries and demonstrated the effectiveness of PCM (Phase Change Material)-based cooling.
- Mahamud and Park (2011) analyzed distributed liquid cooling for EV batteries, showing the cooling performance under varied flow conditions.
- Zhao et al. (2020) compared different TMS designs including heat pipes, liquid plates, and air convection methods for LFP and NMC cells, highlighting LFP's thermal benefits and challenges.

This study distinguishes itself by performing high-resolution simulations on a realistic LFP module geometry under defined operating conditions without the aid of cooling plates or forced airflow.

3. Geometry and Boundary Conditions

The battery module under investigation comprises 23 Lithium Iron Phosphate (LFP) cells connected in series. Each cell is designed to store and deliver electrical energy efficiently, and their series connection ensures that the voltage output is cumulative, meeting the required specifications for the application.

Cell Arrangement and Connections:

- **LFP Cells:** The 23 LFP cells are arranged in a linear configuration, optimizing space and ensuring uniform distribution of electrical load.
- **Aluminum Bus Bars:** These bus bars serve as the electrical connectors between the cells. Aluminum is chosen for its excellent electrical conductivity and lightweight properties, which help in minimizing resistance and enhancing overall efficiency.
- **Series Connection:** The cells are connected in series, meaning the positive terminal of one cell is connected to the negative terminal of the next cell. This arrangement increases the total voltage output while maintaining the same current flow through each cell.
- **Ambient temperature:** 45°C
- **Pressure:** 101325 Pa
- **Gravity:** 9.81 m/s²

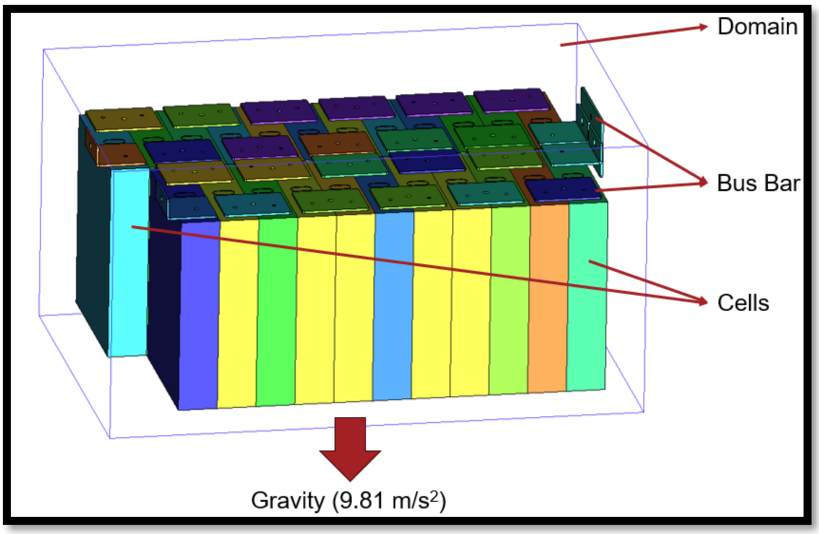

Figure 1: Battery Model

3.1 Calculation of Heat Source for Charging of Battery

Given Data:

1. Battery Voltage (Rating; Voltage under load): **72 V**
2. Individual Cell Voltage: **3.2 V**
3. Single module with **23** cells in series
4. The current passed through the battery pack: **1C 150 Amps**

Calculation of Heat released in single cell:

Consider individual cell resistance as 'r'.

1. Total cell voltage (Open Circuit Voltage, OCV), V = 23 × 3.2 (V) = **73.6 (V)**
2. Voltage drop due to internal resistance, V = $Voltage_{OCV}$ – $Voltage_{under\ load}$ =73.6 (V) – 72 (V) = **1.6 (V)**
3. Internal resistance of the battery pack, R_{eff} = 1.6 (V) / 150 (Amps) = **0.010666 (Ω)**
4. Individual cell resistance of the pack, r = 0.010666 (Ω) / 23 = **0.000463768 (Ω)**
5. Heat released for single cell, Q = I × I × r ; Q = 150 (Amps) × 150 (Amps) × 0.000463768 (Ω) = **10.44 (W)**

For charging, the heat source for single cell is 10.44 W

Total Time for simulation of charging is 60 minutes

3.2 Calculation of Heat Source for Discharging of Battery

Given Data:

1. Battery Voltage (Rating; Voltage under load): **72 V**
2. Individual Cell Voltage**: 3.2 V**
3. Single module with **23** cells in series
4. The current passed through the battery pack: **0.6C 90 Amps**

Calculation of Heat released in single cell:

Consider individual cell resistance as 'r'.

1. Total cell voltage (Open Circuit Voltage, OCV), V = 23 × 3.2 (V) = **73.6 (V)**
2. Voltage drop due to internal resistance, V = $Voltage_{OCV}$ – $Voltage_{under\ load}$;73.6 (V) – 72 (V) = **1.6 (V)**
3. Internal resistance of the battery pack, R_{eff} = 1.6 (V) / 90 (Amps) = **0.0178 (Ω)**
4. Individual cell resistance of the pack, r = 0.0178 (Ω) / 23 = **0.000774 (Ω)**
5. Heat released for single cell, Q = I × I × r ; Q = 90 (Amps) × 90 (Amps) × 0.000774 (Ω) = **6.267 (W)**

For discharging, the heat source for single cell is 6.267 W

For discharge, the total simulation time is 100 minutes

3.3 Numerical Calculation for Charging and Discharging

i. **Data Provided**

- **Battery Pack Voltage**: 72V
- **Battery Pack Capacity**: 150Ah
- **Number of Cells in Series**: 23
- **Voltage per Cell**: 3.2V
- **Charging Current (IC)**: 150A (1C)
- **Discharging Current**: 90A (0.6C)
- **Ambient Temperature**: 45°C

ii. **Single Cell Specifications**

- **Nominal Voltage per Cell**: 3.2V
- **Capacity per Cell**: 150Ah (same as pack)
- **Charging Power per Cell**: Pcharge=Vcell×Icharge=3.2V×150A=480W
- **Discharging Power per Cell**: =Pdischarge=Vcell×Idischarge=3.2V×90A=288W

iii. **Internal Resistance (R)**

Internal resistance causes a voltage drop and heat generation.

Using the formula: $\mathbf{R_{internal} = \Delta V/I}$

The voltage drop ΔV can be estimated from the losses during charging and discharging. We'll assume standard loss values.

iv. **Voltage per Cell**

The voltage of the battery pack is 72V and 23 cells in series:

$V_{cell}=72/23\approx\mathbf{3.13\ V}$

v. **Voltage Drop During Charging**

The nominal voltage of a single cell is 3.2 V. During charging at 150A, the voltage per cell is measured to be 3.13V.

Voltage drop

$\Delta V=3.2-3.13=\mathbf{0.07\ V}$

Internal resistance (Rcell):

$Rcell=\Delta V/I=0.07/150\approx$**0.000467 Ω**

vi. Voltage Drop During Discharging

Assume the voltage during discharging at 90A is the same, 3.13V.

Voltage drop

$\Delta V=3.2-3.13=$**0.07 V**

Internal resistance (Rcell):

$Rcell=\Delta V/I=0.07/90\approx$ **0.000778 Ω**

Heat generation per cell during charging:

$Qheat, charge=I^2charge\cdot Rcell, charge=150^2\cdot 0.000467\approx$**10.51 W.**

Heat generation per cell during discharging:

$Qheat, Discharge=I^2discharge\cdot Rcell, Discharge=90^2\cdot 0.000778\approx$**6.30 W.**

vii. Cell material properties:

- **Density (ρ)**: 2150 kg/m^3
- **Specific heat (cp)**: 550 J/kg
- **Thermal conductivity (k)**: 1.02 W/mK

Charging duration: t=1 hour t =3600 Sec

Discharge Duration=150/90=1.67 Hrs=6000 sec

The cell volume is **0.0014799 m^3**

viii. Cell Mass

The mass of the cell can be calculated using the cell density (ρ=2150 kg/m3) and the provided volume (Vcell=0.0014799m^3):

Mass =2150·0.0014799≈**3.181kg**

ix. Heat Generated During Charging

The heat generated remains the same as previously calculated:

$Q_{heat}=I^2\cdot Rcell\cdot t=150^2\cdot 0.000467\cdot 3600\approx$**37,800J**

- **Temperature Rise**

The temperature rise (ΔT) is calculated as:

$\Delta T=Q_{heat}/m\cdot c_p=37800/3.181*550=21.69^0C+45^0C=$**$66.69^0$C**

x. Heat Generated During Discharging

The heat generated remains the same as previously calculated:

Q_{heat}=I^2·Rcell·t =90^2·0.000778·6000≈**37,707J**

- **Temperature Rise**

The temperature rise (ΔT) is calculated as:

ΔT=Q_{heat}/m·c_p=37707/3.181*550=21.50^{0}C +45^{0}C+66.69^{0}C=**88.19^{0}C**

3.3 Boundary Conditions – Charging

Table 1: Charging Boundary Condition

Analysis Conditions	
Analysis Conditions	Incompressible Turbulent Flow (Standard k-eps model), Heat, Transient Analysis
Basic Settings	Gravity along Negative Y-Axis, Ambient Temperature – 45°C
Source Condition	Apply 10.44 W to the 23 cells
Transient Analysis	Time Step – 1 Second End Time – 3600 (60 minutes)

3.4 Boundary Conditions – Discharging

Table 2: Discharging Boundary Condition

Analysis Conditions	
Analysis Conditions	Incompressible Turbulent Flow (Standard k-eps model), Heat, Transient Analysis
Basic Settings	Gravity along Negative Y-Axis, Ambient Temperature – 45°C
Source Condition	Apply 6.267 W to the 23 cells
Transient Analysis	Time Step – 1 Second End Time – 9600 (60 minutes + 100 minutes)
Restart File	The .r file of charging simulation is used to restart the simulation using the new heat source (discharging heat source)

3.5 Material Properties

Bus Bar – Aluminium 1200

- Density – 2750 Kg/m^3
- Specific Heat – 900 J/kg. K
- Thermal Conductivity – 230 W/m.K

LFP Cell

- Density – 2150 Kg/m^3
- Specific Heat – 550 J/kg.K
- Thermal Conductivity – 1.02 W/m.K

Air

- Density – 1.206 Kg/m^3
- Specific Heat – 1007 J/kg.K
- Thermal Conductivity – 0.0256 W/m.K
- Viscosity – 1.83e-05 Pa.s
- Thermal Expansion Rate – 0.003495 1/K

4. Meshing

The meshing process for the battery module was conducted using SCSTREAM software, which is renowned for its capabilities in computational fluid dynamics (CFD) simulations. The software was utilized to create a structured mesh that accurately represents the geometry and thermal characteristics of the LFP cells within the battery pack.

Structured Mesh:

- **Mesh Configuration:** A structured mesh was employed to ensure precise modeling of the battery cells and their surrounding environment. Structured meshes consist of regular, grid-like patterns that facilitate efficient computation and accurate representation of complex geometries.
- **Cell Coverage:** The mesh was meticulously designed to capture all parts of the cells, including the intricate details at the corners. This comprehensive coverage is essential for accurately predicting temperature variations throughout the cells during charging and discharging cycles.

Temperature Capture:

- **Detailed Resolution:** The structured mesh allows for high-resolution temperature data to be obtained at each corner of the cell. This level of detail is crucial for identifying potential hotspots and understanding the thermal behavior of the battery pack under different operational conditions.

- **Charging and Discharging:** During both charging and discharging processes, the mesh ensures that temperature results are accurately captured, providing insights into how heat is generated and dissipated within the cells.

Mesh Count:

- **Total Mesh Elements:** The total mesh count for the simulation is approximately 635,254 elements. This substantial number of elements reflects the complexity and precision required to model the thermal dynamics of the battery module effectively.

By utilizing SCSTREAM software and implementing a structured mesh, the simulation achieves a high degree of accuracy in predicting temperature evolution within the battery pack. This detailed thermal analysis is essential for designing effective Thermal Management Systems (TMS) that enhance battery performance, safety, and longevity.

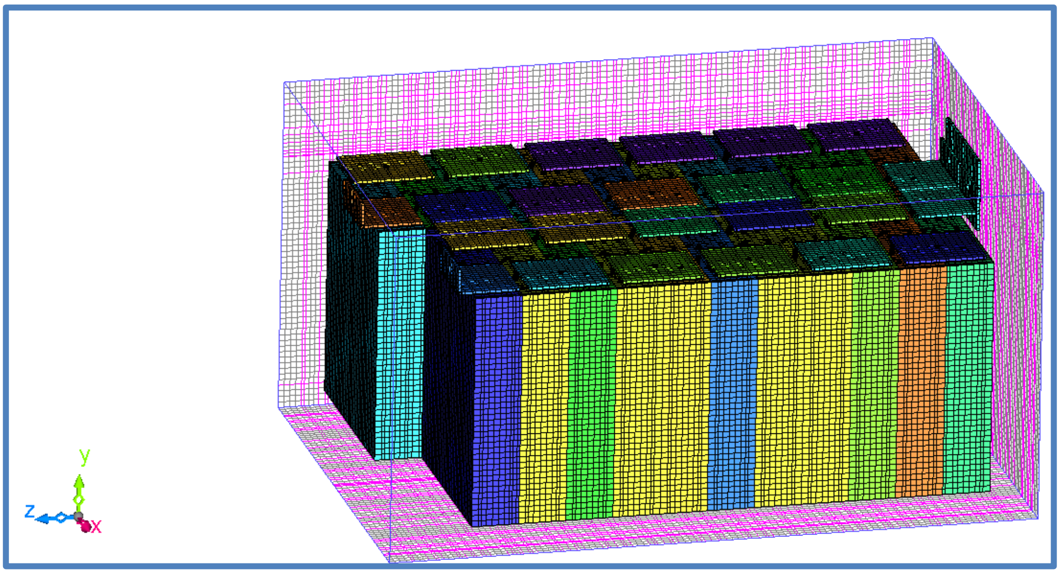

Figure 2: Mesh Model Isometric view

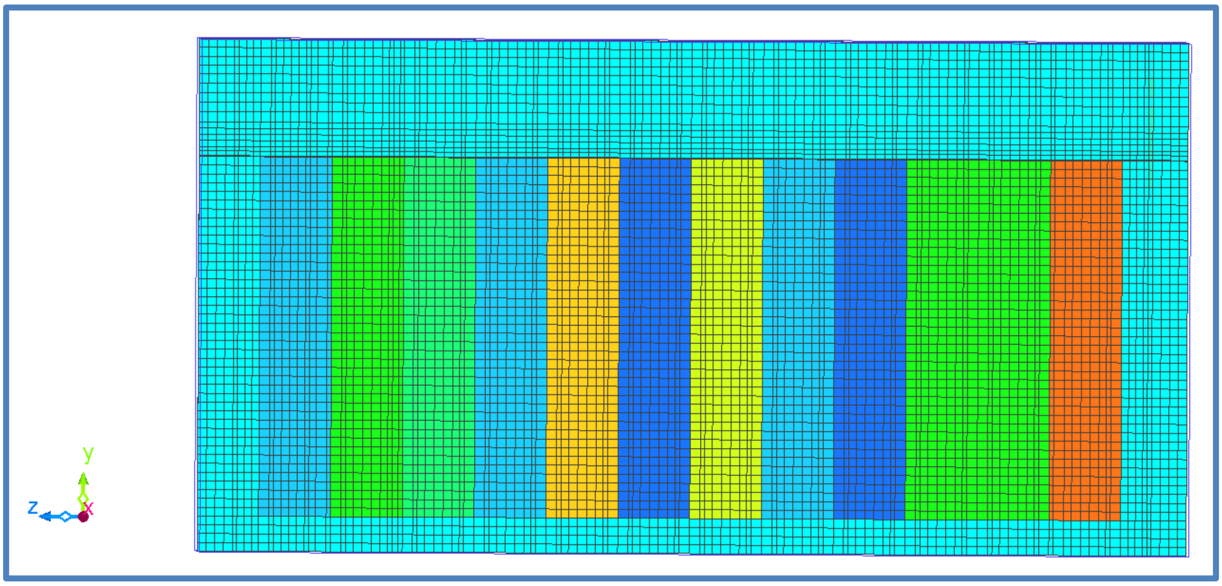

Figure 3: Mesh Model Front view

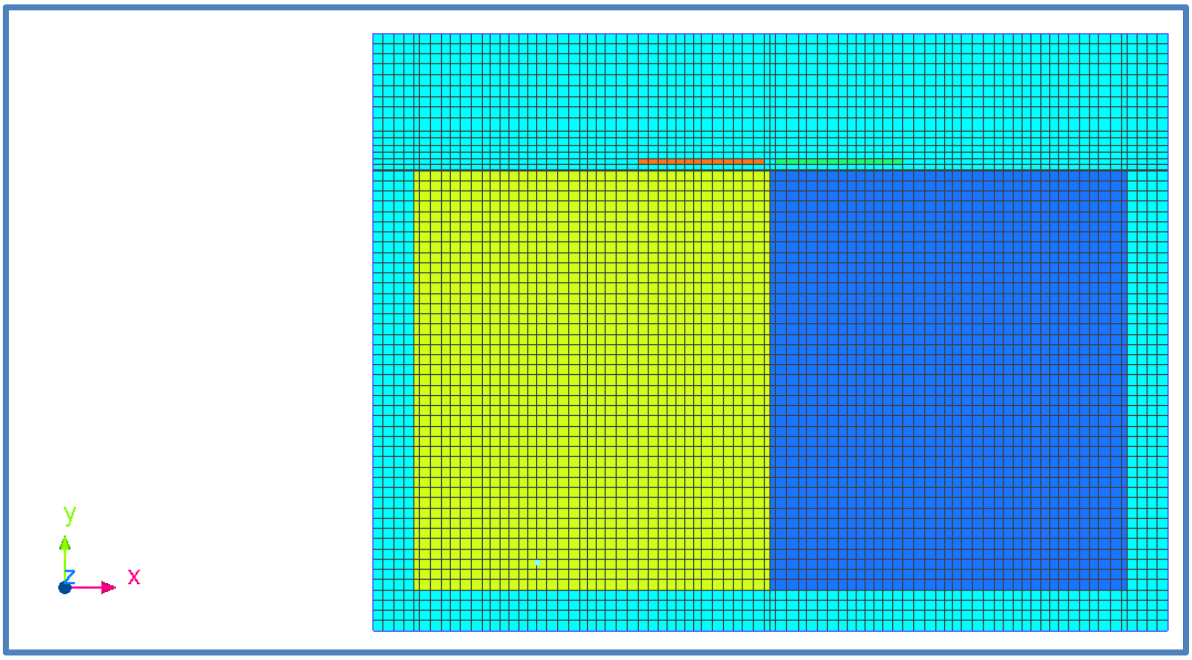

Figure 4: Mesh Model Side view

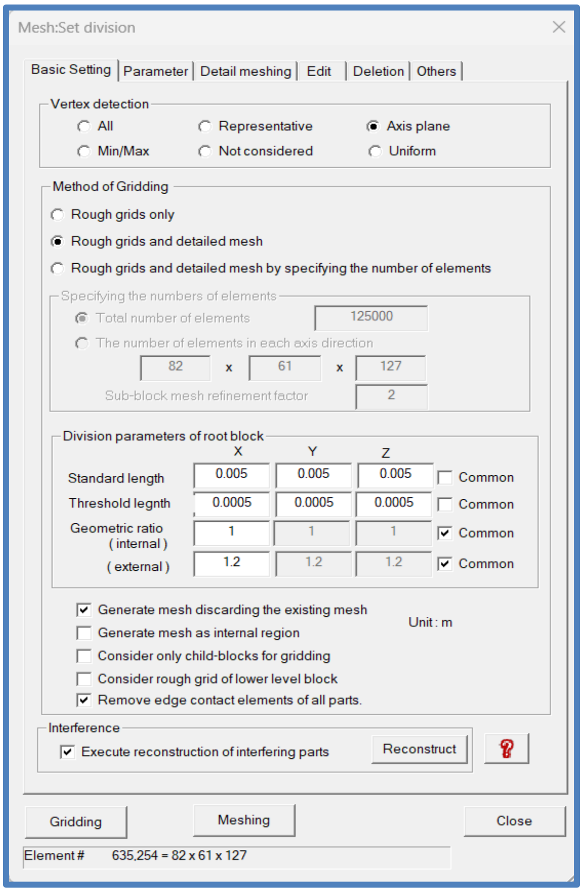

Figure 5: Mesh Conditions

5. Results and Discussion

The temperature contours obtained from the simulation during the charging process revealed significant insights into the thermal behavior of the battery module. The analysis highlighted a peak temperature near the core cells, indicating that heat accumulation was highest in this region. This is primarily due to the increased current flow during charging, which generates more heat within the cells.

Charging Process:

- **Peak Temperature:** During the charging process, the temperatures reached approximately 66.67°C. This peak temperature was observed near the core cells, where the heat generation was most intense.
- **Heat Accumulation:** The core cells experienced higher heat accumulation due to their central position and the higher electrical load they bear. This necessitates effective thermal management to prevent overheating and ensure the longevity of the cells.

Discharging Process:

- **Thermal Gradient:** In contrast, the discharging process exhibited a relatively lower thermal gradient. This is attributed to the reduced current flow and consequently lower heat generation during discharging.
- **Temperature Increase:** Despite the lower thermal gradient, the temperature increased to 88.11°C immediately after the discharge process. This rise in temperature can be attributed to the residual heat from the charging cycle and the continued heat generation during discharging.

Cooling and Convection Effects:

- **Absence of Forced Cooling:** The absence of forced cooling mechanisms, such as fans or liquid cooling, resulted in modest convection effects in the surrounding air. Natural convection alone was insufficient to dissipate the heat effectively, leading to higher temperatures within the cells.
- **Role of Conduction:** The analysis emphasized the significant role of conduction through the aluminum bus bars. The bus bars facilitated heat transfer away from the cells, but their effectiveness was limited without additional cooling strategies.

Numerical Validation:

- **Consistency with Numerical Calculations:** The observed temperatures during both charging and discharging processes were consistent with numerical calculations. This validation underscores the accuracy of the simulation and the reliability of the CFD approach in predicting thermal behavior.

Overall, the detailed thermal analysis underscores the necessity for robust Thermal Management Systems (TMS) to manage heat effectively, especially during fast charging cycles. Future work will focus on integrating forced cooling mechanisms and exploring alternative material configurations to further optimize thermal performance and ensure the safety and efficiency of the battery module.

5.1. Results Charging Temperature Contour

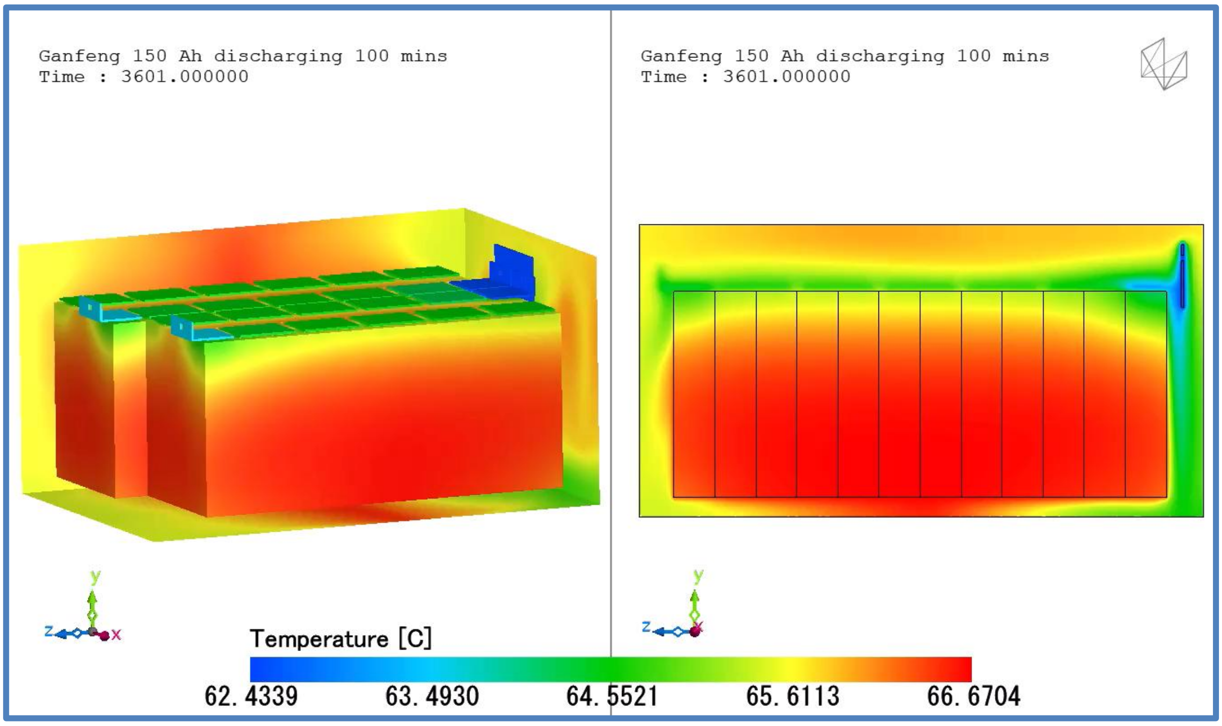

Figure 6: Charging Temperature Contour

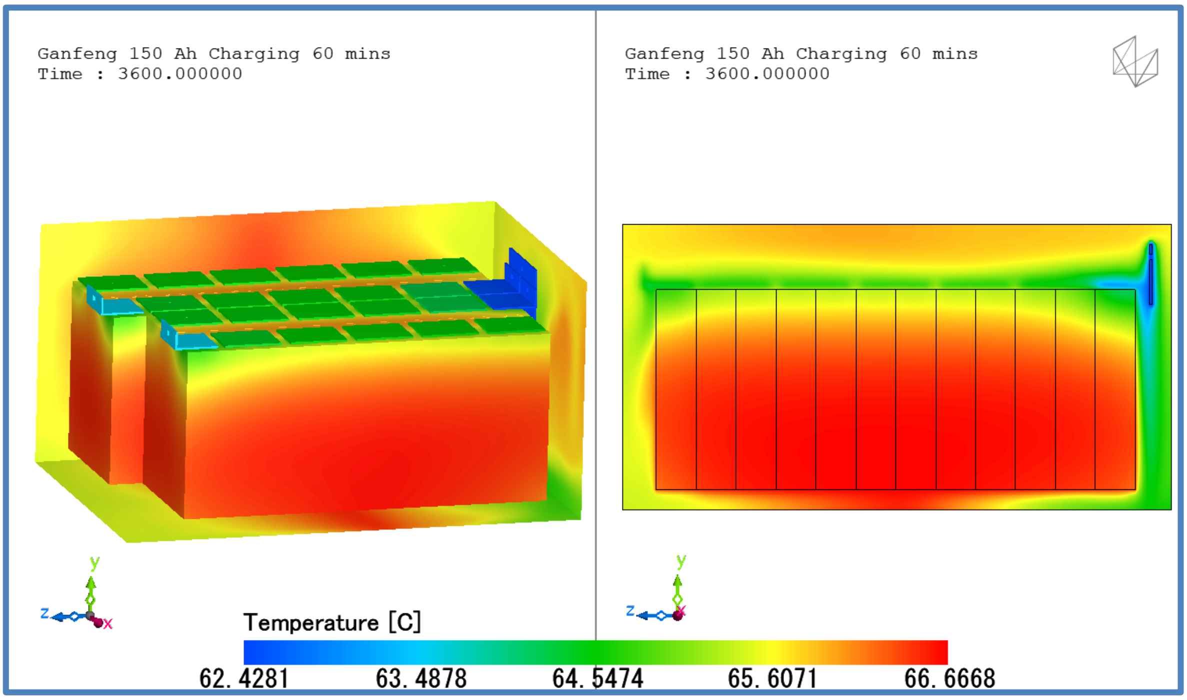

Figure 7: Charging Temperature Contour of different view

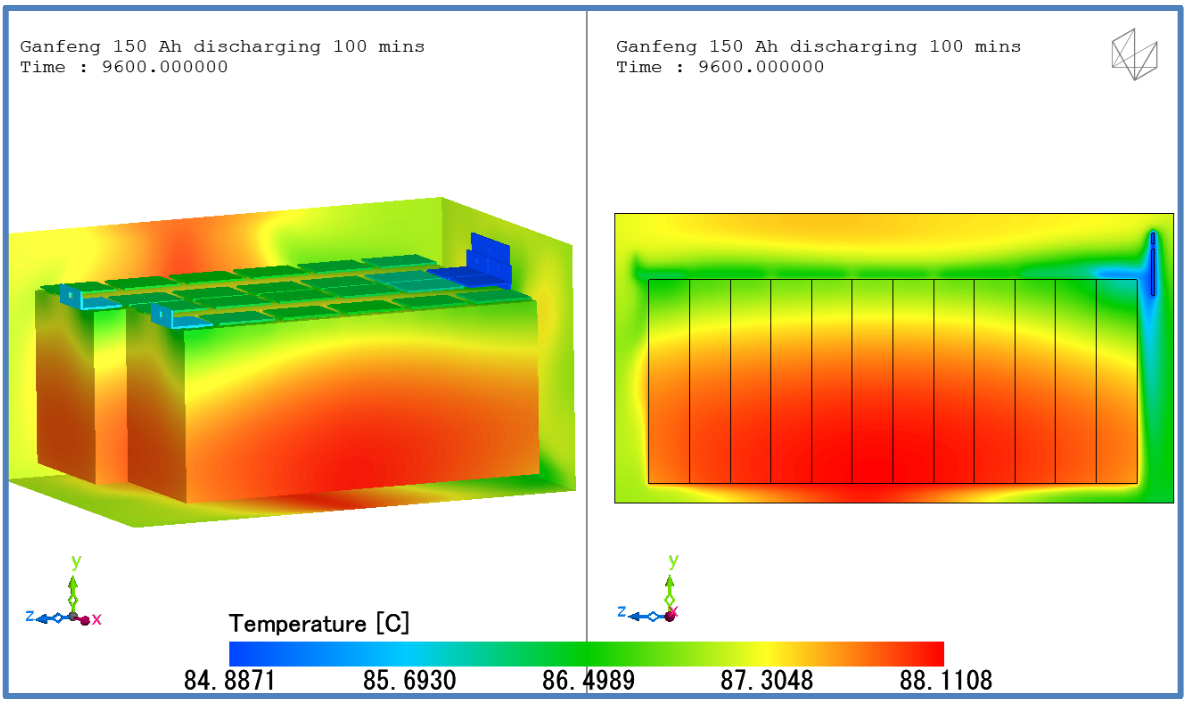

Figure 8: discharging Temperature Contour of different view

5.2 Heat Path Analysis

Clear heat paths were visible along the bus bar-aligned cells, validating the high conductivity of aluminum. Discharging simulations confirmed less aggressive heat spreading compared to the charging scenario.

- **Heat Path View – Charging**

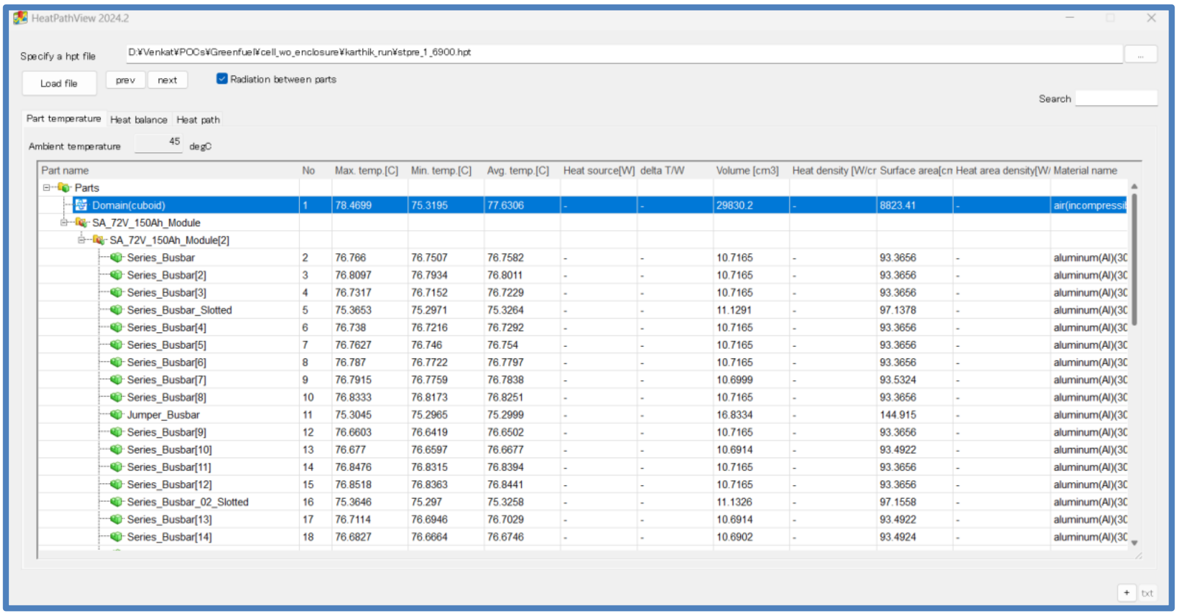

HeatPathView 2024.2

Specify a hpt file D:¥Venkat¥POCs¥Greenfuel¥cell_wo_enclosure¥karthik_run¥stpre_1_6900.hpt

Load file | prev | next | Radiation between parts | Search

Part temperature | Heat balance | Heat path

Ambient temperature 45 degC

Part name	No	Max. temp.[C]	Min. temp.[C]	Avg. temp.[C]	Heat source[W]	delta T/W	Volume [cm3]	Heat density [W/cr	Surface area[cn	Heat area density[W/	Material name
Parts											
Domain(cuboid)	1	78.4699	75.3195	77.6306	-	-	29830.2	-	8823.41	-	air(incompressi
SA_72V_150Ah_Module											
SA_72V_150Ah_Module[2]											
Series_Busbar	2	76.766	76.7507	76.7582	-	-	10.7165	-	93.3656	-	aluminum(Al)(3C
Series_Busbar[2]	3	76.8097	76.7934	76.8011	-	-	10.7165	-	93.3656	-	aluminum(Al)(3C
Series_Busbar[3]	4	76.7317	76.7152	76.7229	-	-	10.7165	-	93.3656	-	aluminum(Al)(3C
Series_Busbar_Slotted	5	75.3653	75.2971	75.3264	-	-	11.1291	-	97.1378	-	aluminum(Al)(3C
Series_Busbar[4]	6	76.738	76.7216	76.7292	-	-	10.7165	-	93.3656	-	aluminum(Al)(3C
Series_Busbar[5]	7	76.7627	76.746	76.754	-	-	10.7165	-	93.3656	-	aluminum(Al)(3C
Series_Busbar[6]	8	76.787	76.7722	76.7797	-	-	10.7165	-	93.3656	-	aluminum(Al)(3C
Series_Busbar[7]	9	76.7915	76.7759	76.7838	-	-	10.6999	-	93.5324	-	aluminum(Al)(3C
Series_Busbar[8]	10	76.8333	76.8173	76.8251	-	-	10.7165	-	93.3656	-	aluminum(Al)(3C
Jumper_Busbar	11	75.3045	75.2965	75.2999	-	-	16.8334	-	144.915	-	aluminum(Al)(3C
Series_Busbar[9]	12	76.6603	76.6419	76.6502	-	-	10.7165	-	93.3656	-	aluminum(Al)(3C
Series_Busbar[10]	13	76.677	76.6597	76.6677	-	-	10.6914	-	93.4922	-	aluminum(Al)(3C
Series_Busbar[11]	14	76.8476	76.8315	76.8394	-	-	10.7165	-	93.3656	-	aluminum(Al)(3C
Series_Busbar[12]	15	76.8518	76.8363	76.8441	-	-	10.7165	-	93.3656	-	aluminum(Al)(3C
Series_Busbar_02_Slotted	16	75.3646	75.297	75.3258	-	-	11.1326	-	97.1558	-	aluminum(Al)(3C
Series_Busbar[13]	17	76.7114	76.6946	76.7029	-	-	10.6914	-	93.4922	-	aluminum(Al)(3C
Series_Busbar[14]	18	76.6827	76.6664	76.6746	-	-	10.6902	-	93.4924	-	aluminum(Al)(3C

Figure 9: Heat Path view information of each part during Charging cycle

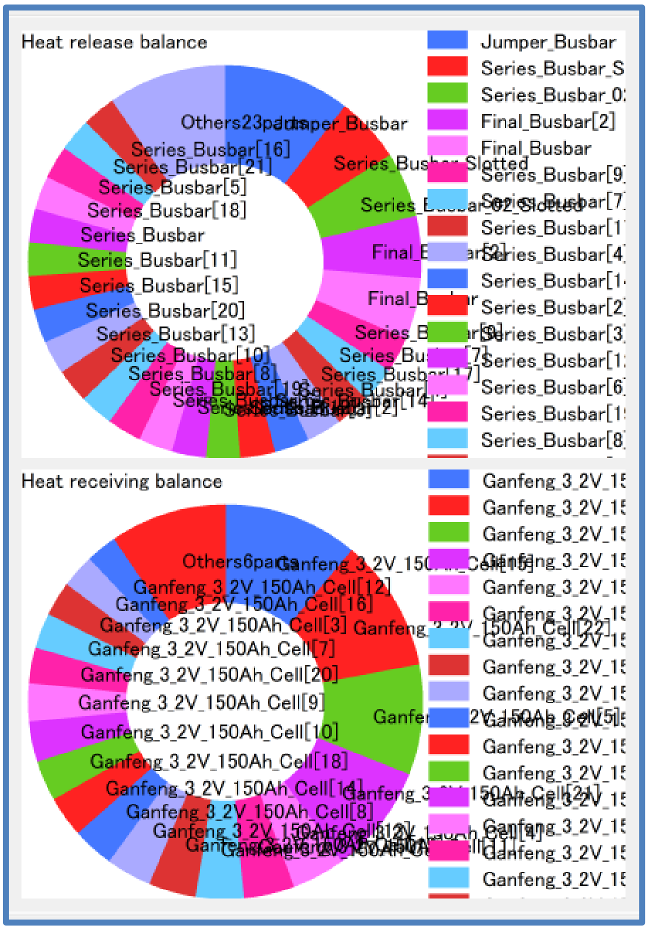

Figure 10: Heat balance information of each part during Charging cycle

- **Heat Path View – Discharging**

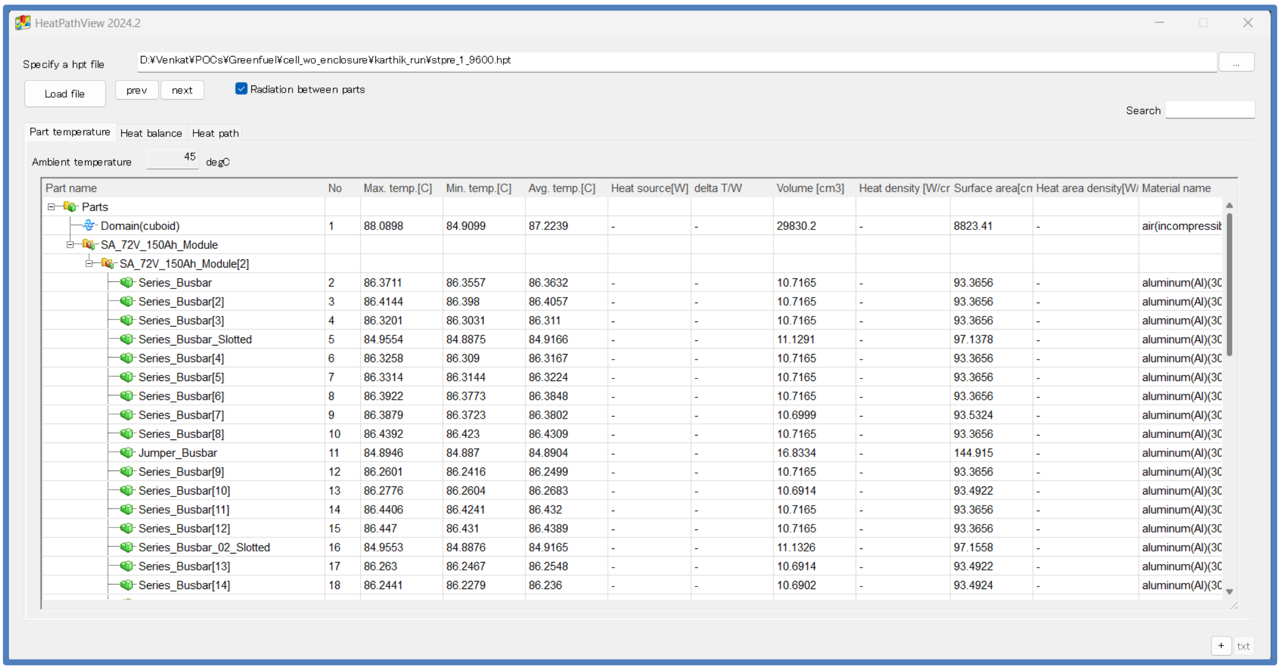

HeatPathView 2024.2

Specify a hpt file D:¥Venkat¥POCs¥Greenfuel¥cell_wo_enclosure¥karthik_run¥stpre_1_9600.hpt

Load file | prev | next | Radiation between parts

Search

Part temperature | Heat balance | Heat path

Ambient temperature 45 degC

Part name	No	Max. temp.[C]	Min. temp.[C]	Avg. temp.[C]	Heat source[W]	delta T/W	Volume [cm3]	Heat density [W/cr	Surface area[cn	Heat area density[W/	Material name
Parts											
Domain(cuboid)	1	88.0898	84.9099	87.2239	-	-	29830.2	-	8823.41	-	air(incompressit
SA_72V_150Ah_Module											
SA_72V_150Ah_Module[2]											
Series_Busbar	2	86.3711	86.3557	86.3632	-	-	10.7165	-	93.3656	-	aluminum(Al)(3C
Series_Busbar[2]	3	86.4144	86.398	86.4057	-	-	10.7165	-	93.3656	-	aluminum(Al)(3C
Series_Busbar[3]	4	86.3201	86.3031	86.311	-	-	10.7165	-	93.3656	-	aluminum(Al)(3C
Series_Busbar_Slotted	5	84.9554	84.8875	84.9166	-	-	11.1291	-	97.1378	-	aluminum(Al)(3C
Series_Busbar[4]	6	86.3258	86.309	86.3167	-	-	10.7165	-	93.3656	-	aluminum(Al)(3C
Series_Busbar[5]	7	86.3314	86.3144	86.3224	-	-	10.7165	-	93.3656	-	aluminum(Al)(3C
Series_Busbar[6]	8	86.3922	86.3773	86.3848	-	-	10.7165	-	93.3656	-	aluminum(Al)(3C
Series_Busbar[7]	9	86.3879	86.3723	86.3802	-	-	10.6999	-	93.5324	-	aluminum(Al)(3C
Series_Busbar[8]	10	86.4392	86.423	86.4309	-	-	10.7165	-	93.3656	-	aluminum(Al)(3C
Jumper_Busbar	11	84.8946	84.887	84.8904	-	-	16.8334	-	144.915	-	aluminum(Al)(3C
Series_Busbar[9]	12	86.2601	86.2416	86.2499	-	-	10.7165	-	93.3656	-	aluminum(Al)(3C
Series_Busbar[10]	13	86.2776	86.2604	86.2683	-	-	10.6914	-	93.4922	-	aluminum(Al)(3C
Series_Busbar[11]	14	86.4406	86.4241	86.432	-	-	10.7165	-	93.3656	-	aluminum(Al)(3C
Series_Busbar[12]	15	86.447	86.431	86.4389	-	-	10.7165	-	93.3656	-	aluminum(Al)(3C
Series_Busbar_02_Slotted	16	84.9553	84.8876	84.9165	-	-	11.1326	-	97.1558	-	aluminum(Al)(3C
Series_Busbar[13]	17	86.263	86.2467	86.2548	-	-	10.6914	-	93.4922	-	aluminum(Al)(3C
Series_Busbar[14]	18	86.2441	86.2279	86.236	-	-	10.6902	-	93.4924	-	aluminum(Al)(3C

Figure 11: Heat path view information of each part during discharging cycle

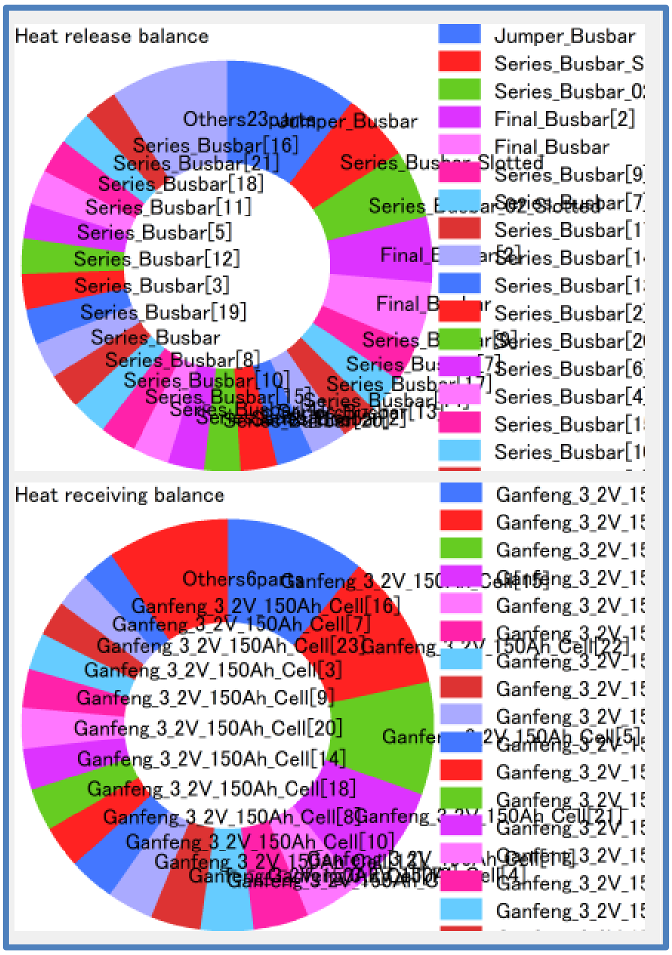

Figure 12: Heat balance information of each part during discharging cycle

Conclusion

1. The simulation underscores the critical importance of implementing robust Thermal Management Systems (TMS), especially during fast charging cycles. Fast charging can significantly elevate internal temperatures due to increased current flow, which, if not properly managed, can lead to thermal runaway and reduced battery lifespan.
2. The findings from this study affirm the efficacy of Computational Fluid Dynamics (CFD) tools in accurately resolving internal pack temperatures. This capability is crucial for identifying potential hotspots and guiding design improvements to enhance overall battery safety and performance.
3. The results of the simulation demonstrate that CFD can effectively model the thermal behavior of battery packs under various operational conditions.

4. This modeling provides valuable insights into how different design parameters and cooling strategies impact temperature distribution within the pack.
5. By comparing the charging and discharging results with numerical calculations, the study validates the accuracy of the CFD approach, reinforcing its utility in battery thermal management research.
6. Future work will focus on further optimizing battery performance by integrating forced cooling mechanisms and exploring alternative material configurations.
7. Forced cooling, such as liquid or air cooling, can significantly enhance heat dissipation, maintaining optimal operating temperatures even during high-demand scenarios.
8. Additionally, experimenting with different materials for battery components can lead to improved thermal conductivity and reduced internal resistance, further enhancing the efficiency of the TMS.
9. Overall, this research highlights the potential of CFD as a powerful tool for advancing battery technology. By providing a detailed understanding of thermal dynamics, CFD can guide the development of more effective and reliable TMS, ultimately contributing to the creation of safer and longer-lasting lithium-ion batteries.

Acknowledgments

We would like to extend our sincere gratitude to **Hexagon Manufacturing Intelligence** for providing their **Cradle CFD SCStream** software. Utilizing this advanced simulation tool has enabled us to achieve superior results compared to traditional numerical calculations. Your support has been invaluable in enhancing the accuracy and efficiency of our simulations.

Thank you for your continued partnership and contribution to our success.

References

[1] Rao, Z., et al. (2014). "Thermal analysis of a battery pack using CFD simulation." Applied Thermal Engineering.

[2] Al-Zareer, M., et al. (2018). "Electro-thermal modeling and analysis of LFP battery systems." Journal of Power Sources.

[3] Wang, Y., et al. (2021). "Thermal behavior of cylindrical lithium-ion cells and its impact on pack design." Energy Reports.

[4] Kim, G.H., et al. (2017). "Cooling performance of a passive air cooling system for lithium-ion battery packs." Journal of Power Sources, 342, 232–243.

[5] Yang, X.G., et al. (2018). "Modeling the coupled electrochemical and thermal behavior of prismatic lithium-ion batteries." Electrochimica Acta, 282, 618–628.

[6] Mahamud, R., Park, C. (2011). "Recirculation cooling for lithium-ion battery packs." Applied Thermal Engineering, 31(14–15), 2145–2152.

[7] Zhao, R., et al. (2020). "Review of thermal management of lithium-ion batteries for electric vehicles." Energy Storage Materials, 24, 644–667.

Citation: Karthik A V, Balaji S, Venkat S G, Muralidhar Reddy. (2025). Thermal Simulation of LFP Battery Module During Charging and Discharging Cycles Using CFD. International Journal of Mechanical Engineering and Technology (IJMET), 16(3), 88-105.

Abstract Link: https://iaeme.com/Home/article_id/IJMET_16_03_005

Article Link:
https://iaeme.com/MasterAdmin/Journal_uploads/IJMET/VOLUME_16_ISSUE_3/IJMET_16_03_005.pdf

✉ **editor@iaeme.com**